

Spatio-Temporal Low Count Processes with Application to Violent Crime Events

Sivan Aldor-Noiman Lawrence D. Brown Emily B. Fox
Robert A. Stine

April 23, 2013

Abstract

There is significant interest in being able to predict where crimes will happen, for example to aid in the efficient tasking of police and other protective measures. We aim to model both the temporal and spatial dependencies often exhibited by violent crimes in order to make such predictions. The temporal variation of crimes typically follows patterns familiar in time series analysis, but the spatial patterns are irregular and do not vary smoothly across the area. Instead we find that spatially disjoint regions exhibit correlated crime patterns. It is this indeterminate inter-region correlation structure along with the low-count, discrete nature of counts of serious crimes that motivates our proposed forecasting tool. In particular, we propose to model the crime counts in each region using an integer-valued first order autoregressive process. We take a Bayesian nonparametric approach to flexibly discover a clustering of these region-specific time series. We then describe how to account for covariates within this framework. Both approaches adjust for seasonality. We demonstrate our approach through an analysis of weekly reported violent crimes in Washington, D.C. between 2001-2008. Our forecasts outperform standard methods while additionally providing useful tools such as prediction intervals.

Keywords: Violent crime counts, Low-count time series, INAR, Bayesian nonparametric methods

1 Introduction

Violent crimes are a significant concern in metropolitan areas across the United States. The impact of violent crimes on a city are many fold, ranging from harm to residents to loss of tourism, and the ability to curb such crimes is of utmost importance. In particular, there is significant interest in being able to predict regions in which crimes are likely to occur so

that preventive measures may be employed in both the short- and long-term. Predicting crimes relies on the presence of dependence over time and among regions. The structure of the temporal dependence we find is familiar; for example, violent crimes are known to vary seasonally, with the rate of violent crimes higher during warmer months of the year (McDowall et al., 2012). The spatial dependence is more complex. One might expect, for instance, neighboring regions to experience similar crime rates. Geographic features, however, can impede crime from varying smoothly across regions. For example in Washington, D.C., Rock Creek Park in the northeast and the Anacostia River in the south create natural impediments to the spread of crime. Boundaries also occur at a finer resolution (e.g. railroad tracks and highways). The presence of such idiosyncratic features makes it challenging to devise statistical models that are able to borrow strength among similar local regions without over-smoothing distinct regions.

As an example of our methodology, we consider rates of violent crimes in the 188 census tracts in Washington, D.C.. The nation’s capital has consistently ranked among the top cities for rates of violent crimes in the United States. The crimes in our data consist of rape, robbery, arson and aggravated assault. Along with murder, these types of crimes define the FBI part 1 violent crimes list. Part 1 crimes are considered serious and are directly reported to the police (as opposed to other law agencies such as the IRS). Indeed, the Washington, D.C. police department keeps a record of all reported type 1 violent crimes and makes it publicly available through their website (<http://crimemap.dc.gov/CrimeMapSearch.aspx>).

Figure 1 (left) shows a map of Washington, D.C. with boundaries of the census tracts superimposed. The sizes of the census tracts vary widely depending on population density. A census tract consists of adjacent street blocks selected to be homogeneous with respect to demographic features such as economic status and living conditions. According to the 2000 Census, tracts in Washington, D.C. average 3043 residents, ranging from 149 to 7278. Due to the demographic homogeneity of census tracks, it is not surprising that neighboring tracts

often have different crime dynamics.

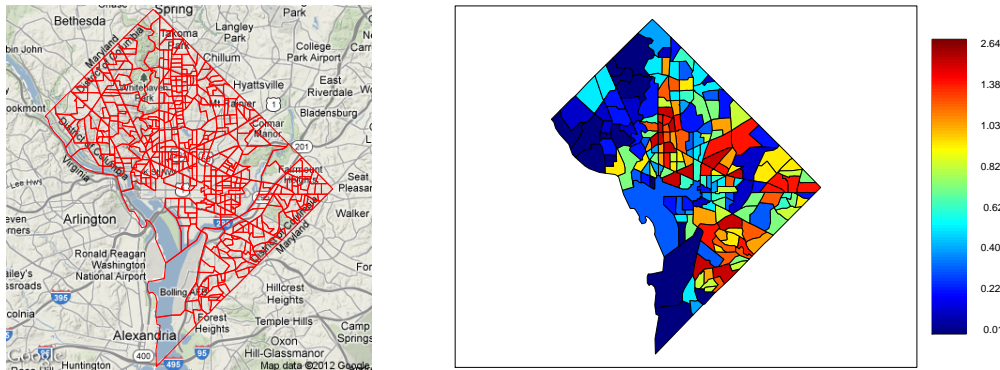


Figure 1: *Left:* Map of the 188 census tracts in Washington, D.C.. *Right:* Weekly average violent crime counts across the 188 census tracts.

The combination of demographic heterogeneity and natural boundaries contributes to the spatially diverse crime patterns across the census tracts. Figure 1 (right) shows the weekly average counts of violent crimes in Washington, D.C. between 2001 and 2008. This plot reveals several interesting features. First, the weekly average number of violent crimes are (fortunately) low. Second, tracts with similar average crime counts are often quite spatially disjoint. This suggests that crime, as hypothesized, does not vary smoothly across the city.

The seasonal structure of weekly crime counts is difficult to see in sequence plots of the data for a single tract because of the small counts. The pattern becomes evident, however, in the aggregate. Figure 2 displays monthly crime counts accumulated over all of the tracts. This plot reveals the seasonal peaks and valleys. (Supplementary Material Section E includes plots of the counts for individual tracts.) Figure 2 also shows summary statistics accumulated over time for the individual tracts. In particular, it shows the distribution of the total counts per tract over these years and a graph of the within-tract standard deviation versus the mean for all tracts.

The features of the weekly crime time series, namely (i) low-count discrete data with (ii) an uncertain correlation structure, necessitate the development of new forecasting tools. In particular, we propose a novel methodology which models each regional time series as

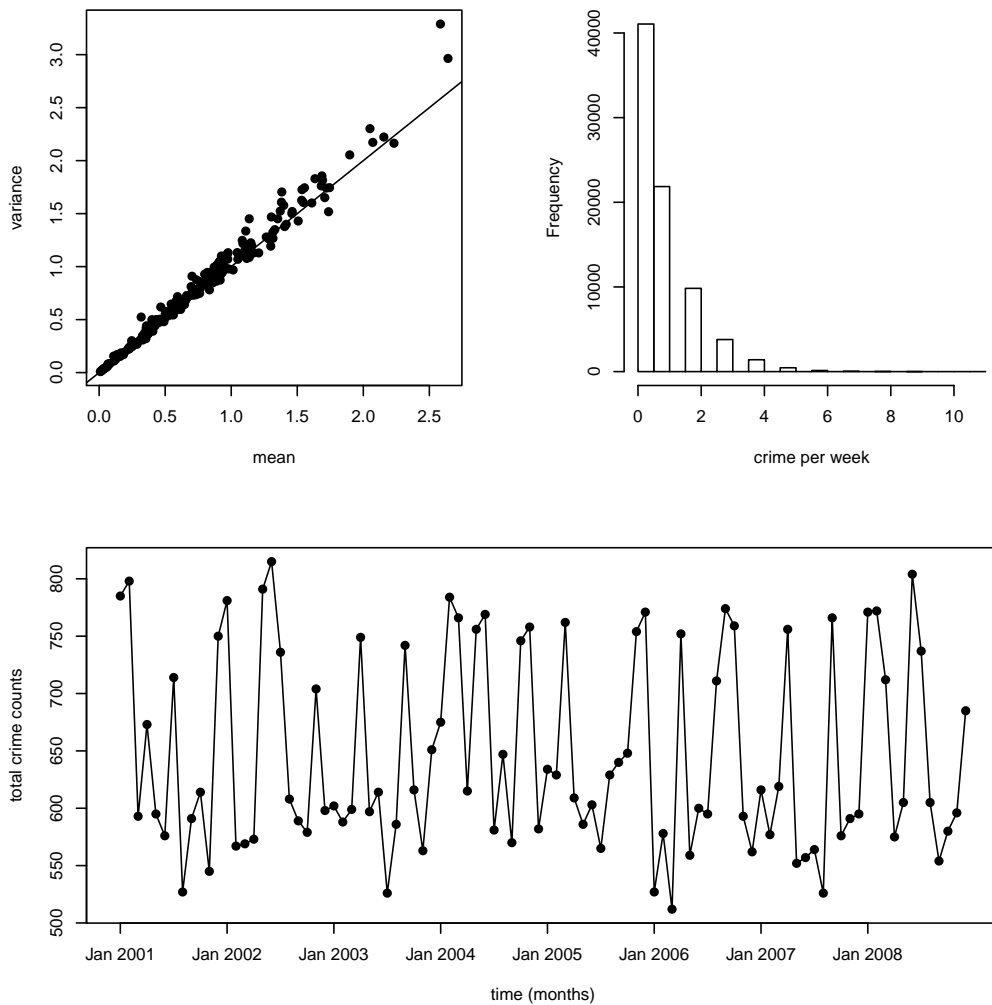


Figure 2: *Top Left:* Histogram of weekly crime rates in Washington, D.C.’s 188 census tracts. *Top Right:* Weekly standard deviation versus average violent crime counts across the 188 census tracts. *Bottom Right:* Total monthly crime counts.

an integer-valued first-order autoregressive process (INAR(1)) (Alzaid and Al-Osh, 1988, McKenzie, 2000). We induce correlation between the time series through the innovations of the INAR(1) models. We decompose these innovation processes into two latent factors: a shared seasonal effect and a rate function which is tract specific. We use multiple shrinkage to cope with the large number of tracts. We obtain this shrinkage adaptively by adopting a nonparametric Bayesian approach that imposes a Dirichlet process prior on the tract

rates. The Dirichlet process leads to a clustering of rates and thus efficient sharing of the information between tracts in a flexible, data-driven manner.

We begin in Section 3 with a purely geographic approach that is aligned with police procedures and work solely with raw crime counts within census tracts. We then examine how to account for covariates, in particular population size, in Section 7.

We develop an efficient Markov chain Monte Carlo scheme for fitting these models, and we use this scheme to fit our model to simulated and real data. The results demonstrate that our proposed multivariate INAR(1) model produces out-of-sample forecasts that are more accurate than those of a conditional least-squares (CLS) model in both simulations and when predicting crimes in Washington, D.C.. One reasonable explanation as to why our model outperforms CLS is because the number of clusters discovered is small relative to the number of tracts. Our model essentially shrinks the time series estimators that share a rate toward a common mean, thereby yielding better out-of-sample forecasts. Another advantage, a byproduct of the Bayesian framework, is that the Bayesian model provides posterior distributions of the p -step-ahead forecasts. These distributions are important in the context of forecasting crime because the distribution of crime is right-skewed and decision makers often care about preparing for the worst-case scenario. Prediction intervals for the number of violent crimes in each region can help the police distinguish between an unusual rise in violent crimes that requires intervention and a rise which is due to random variation.

1.1 Related Approaches

Multivariate Poisson-based models are a natural match to spatio-temporal time series of counts, and this structure has been employed in various prior applications. For example, Boudreault and Charpentier (2011) model the occurrences of earthquakes using a maximum likelihood approach to infer the model parameters of a multivariate INAR(1) process with Poisson innovations. (This formulation does not maintain Poisson margins, as discussed

in Section 2.) Taddy (2010) employed Poisson processes to track the intensity of violent crimes in Cincinnati and treats these as point processes. Taddy (2010) factors the spatial Poisson rate into a process density, modeled using Bayesian nonparametrics, and an overall intensity. Both were allowed to evolve in time. Such a formulation, however, assumes spatial smoothness to the crime rates. Additionally, Taddy (2010) focus on in-sample inference rather than on predicting future events. In contrast, our research focuses on areal data modeling and provides methods to forecast these as multiple integer-valued low-count time series. We harness the efficient and elegant structure of INAR(1) processes and present a method for modeling multiple, correlated time series while maintaining Poisson margins. The correlations are induced via a Bayesian nonparametric clustering of the time series, and in doing so, we efficiently share information to produce more accurate out-of-sample predictions. Bayesian nonparametric methods have previously been studied as tools for data-driven clustering analysis (cf., Dorazio et al., 2008, Fox et al., 2010, Teh et al., 2006). However, these studies focus on clustering either continuous-valued time series or Poisson counts which have no time component.

Our paper is structured as follows. In Section 2, we provide background on the Poisson INAR(1). We then present our method for correlating multiple such processes while maintaining Poisson margins in Section 3. Here, our focus is on correlation structure captured by geography alone. The associated posterior computations via Markov chain Monte Carlo are detailed in Section 4. In Section 5, we briefly provide a simulation study and in Section 6, we analyze our crime data of interest. Finally, in Section 7 we describe a method for accounting for covariates, and in particular consider population size as a predictor.

2 Univariate PoINAR(1) Background

A univariate PoINAR(1) model is defined as follows (Alzaid and Al-Osh, 1988):

$$Y_{t+1} = \alpha \circ Y_t + \epsilon_{t+1} \quad \text{for } t = 0, 1, 2, \dots, \quad (1)$$

where the innovations $\{\epsilon_t\}$ are iid Poisson. The operator \circ denotes binomial thinning. For any nonnegative integer-valued random variable X and for any $\alpha \in [0, 1]$, the random variable $\alpha \circ X$ is defined

$$\alpha \circ X = \sum_{i=1}^X B_i(\alpha), \quad (2)$$

where $B_i(\alpha)$ are independent, identically distributed Bernoulli random variables with success probability α . Given a Poisson distribution on the initial state Y_0 with finite mean $\mu = E Y_0$ and independence between Y_t and $\epsilon_t \sim \text{Poisson}((1 - \alpha)\mu)$, the construction Eq. (1) yields a strongly stationary process. In essence, to obtain a stationary Poisson marginal distribution from Eq. (1), the innovations must also be Poisson (Alzaid and Al-Osh, 1988, Steutel and Van Harn, 1986, Wolpert and Brown, 2011).

3 Multivariate PoINAR(1)

In this section we define a multivariate INAR process that retains Poisson margins. We first introduce the basic model and then demonstrate how to induce correlations among the component series by placing a Dirichlet process prior on the rate parameters of the Poisson innovations. We conclude this section by highlighting the similarities and differences between the proposed model and the vector autoregressive process, which is the equivalent model with Gaussian margins.

Throughout, let $Y_{l,t}$ denote the number of violent crimes at tract $l = 1, \dots, L$ during week $t = 1, \dots, T$. Furthermore, let $\mathbf{Y}_t := (Y_{1,t}, \dots, Y_{L,t})$ denote a vector of crime counts at time

t and $\boldsymbol{\epsilon}_t := (\epsilon_{1,t}, \epsilon_{2,t}, \dots, \epsilon_{L,t})$ the vector of innovations.

3.1 A multivariate PoINAR(1) process

One might imagine employing a multivariate PoINAR(1) analogue of a vector autoregressive process by simply considering:

$$\mathbf{Y}_{t+1} = \boldsymbol{\alpha} \circ \mathbf{Y}_t + \boldsymbol{\epsilon}_{t+1} .$$

where α is an $L \times L$ matrix with entries in $[0, 1]$ and $\boldsymbol{\alpha} \circ \mathbf{Y}_t$ is defined as:

$$[\boldsymbol{\alpha} \circ \mathbf{Y}]_{i,t} := \sum_{l=1}^L \alpha_{i,l} \circ Y_{l,t}, \quad (3)$$

with $\alpha_{i,l} \circ Y_{l,t}$ defined by the binomial thinning operator Eq. (2). Even in the simplest scenario of $\epsilon_{i,t}$ being independent Poisson innovations, however, the resulting margins are in general not Poisson. In fact, it is straightforward to prove that when the off-diagonal elements of the thinning matrix $\boldsymbol{\alpha}$ are non-zero, a stationary distribution exists but is no longer the Poisson distribution (See McKenzie, 2000, Pedeli and Karliss, 2011). Such a multivariate INAR(1) was considered in (Boudreault and Charpentier, 2011).

The one scenario in which Poissonicity is maintained is if $\boldsymbol{\alpha}$ is diagonal, *i.e.* $\alpha_{i,j} = 0$ for $i \neq j$, so that the model becomes

$$\begin{pmatrix} Y_{1,t+1} \\ Y_{2,t+1} \\ \vdots \\ Y_{L,t+1} \end{pmatrix} = \begin{pmatrix} \alpha_1 & 0 & \dots & 0 \\ 0 & \alpha_2 & \dots & 0 \\ \vdots & \vdots & \ddots & \vdots \\ 0 & \dots & 0 & \alpha_L \end{pmatrix} \circ \begin{pmatrix} Y_{1,t} \\ Y_{2,t} \\ \vdots \\ Y_{L,t} \end{pmatrix} + \begin{pmatrix} \epsilon_{1,t+1} \\ \epsilon_{2,t+1} \\ \vdots \\ \epsilon_{L,t+1} \end{pmatrix}. \quad (4)$$

For notational convenience we will denote the diagonal elements by $\alpha_i := \alpha_{i,i}$. The diagonal thinning matrix implies that at time t , the l^{th} entry of the thinned random vector is only a

function of only the l^{th} tract:

$$[\boldsymbol{\alpha} \circ \mathbf{Y}_t]_l = \alpha_l \circ Y_{l,t}. \quad (5)$$

For the innovations processes, we assume $\epsilon_{l,t} | \Lambda_{l,t} \sim \text{Poisson}(\Lambda_{l,t})$. That is, conditional on the rate parameters, the innovations are independently Poisson distributed across time and space. The resulting multivariate INAR(1) yields a stationary Poisson distribution for each element in \mathbf{Y}_t . We refer to this process as the *multivariate PoINAR(1)*. We emphasize that the diagonal thinning matrix not only dramatically reduces the number of model parameters, but also produces a stationary process with Poisson margins.

Conditioning on the rate parameters $\{\Lambda_{l,t}\}$ yields L independent time series. To allow such models to capture dependencies between the time series, we introduce a Dirichlet process mixture model for the innovations in the next section.

3.2 Capturing dependencies

There are several ways to induce dependencies between the elements of the multivariate PoINAR(1) process. As previously mentioned, there are two sources of variation in the model: the multivariate binomial thinning operator and the innovation process. We propose to generate the dependence through the innovations and assume that the binomial thinning operators are independent across the time series. For our model of crime rates, this formulation shares information between tracts while allowing tract-dependent autocorrelations. Furthermore, this focus on the innovations provides computational efficiencies as described in Section 4.

Recall that the innovations are assumed to follow a Poisson distribution with rates $\Lambda_{l,t}$. The rate is a function of both the tract l and the time period t of the specific innovation $\epsilon_{l,t}$.

We decompose the rate $\Lambda_{l,t}$ into a product of a spatial and temporal components:

$$\Lambda_{l,t} = \lambda_l \theta_{s(t)}, \tag{6}$$

where the summands are

- a tract-specific rate, λ_l , and
- a seasonal monthly rate, $\theta_{s(t)}$, that is spatially homogeneous. Here, $s(t)$ is a function that maps week t to its associated month. That is, we assume a constant seasonal effect within months and model this effect with 12 parameters $\theta_1, \dots, \theta_{12}$.

The resulting model for the innovations can be written as follows:

$$\epsilon_{l,t} \sim \text{Poisson}(\lambda_l \theta_{s(t)}). \tag{7}$$

The temporal component induces some dependence across tracts because it is shared across the different time series. A Dirichlet process (DP) prior on the rates, λ_l , provides the balance of the dependence.

The Dirichlet process, denoted $\text{DP}(\tau, G_0)$, provides a distribution over countably infinite probability measures. G_0 denotes a probability distribution over some space Ω ; in our application, Ω is the positive real line. The concentration parameter $\tau > 0$ controls the ‘clumpyness’ of the process. A Dirichlet process can be written as a weighted sum of point masses δ_x positioned by randomly sampling G_0 :

$$G = \sum_{k=1}^{\infty} \beta_k \delta_{\phi_k}, \quad \phi_k \stackrel{iid}{\sim} G_0. \tag{8}$$

The weights β_k can be obtained sequentially via the so-called *stick-breaking* construction

(Sethuraman, 1994):

$$\beta_k = \nu_k \prod_{l=1}^{k-1} (1 - \nu_l) \quad \nu_k \sim \text{Beta}(1, \tau). \quad (9)$$

In effect, the process divides the unit interval into segments with lengths given by the decreasing sequence of weights β_k : the k^{th} weight is a random proportion ν_k of the segment that remains after the first $k - 1$ weights have been chosen. We denote this distribution by $\beta \sim \text{GEM}(\tau)$.

The DP has proven useful in many applications due to its clustering properties (cf., Teh et al., 2006). The *predictive distribution* of draws $W \sim G$ shows why the DP produces clusters. Because probability measures drawn from a DP are discrete by construction, there is a strictly positive probability of multiple observations of W taking identical values within the set $\{\phi_k\}$, with ϕ_k defined as in Eq. (8). For each sampled observation w_i , let z_i identify the position of the corresponding parameter ϕ_k such that $w_i = \phi_{z_i}$. The predictive distribution on the membership variables can be written in the following manner:

$$Z_{N+1} | (z_1, \dots, z_N, \tau) = \begin{cases} K + 1 & \text{w.p. } \frac{\tau}{N + \tau} \\ k & \text{w.p. } \frac{n_k}{N + \tau} \text{ for } k = 1, \dots, K, \end{cases} \quad (10)$$

where n_k indicates the number of members belonging to the k^{th} group and $K = \max\{z_1, \dots, z_N\}$ identifies the number of distinct values observed through the first N samples. The distribution on partitions induced by the sequence of conditional distributions in Eq. (10) is commonly referred to as the *Chinese restaurant process* (CRP). The CRP provides an alternative representation to the DP (Pitman, 2006). This representation emphasizes the reinforcement property of the DP that leads to its clustering properties. It can be shown that the expected number of clusters using the CRP grows as $O(\tau \log(L))$ where L is the number of observations (see Teh, 2011, for a detailed proof.). This implies that the average

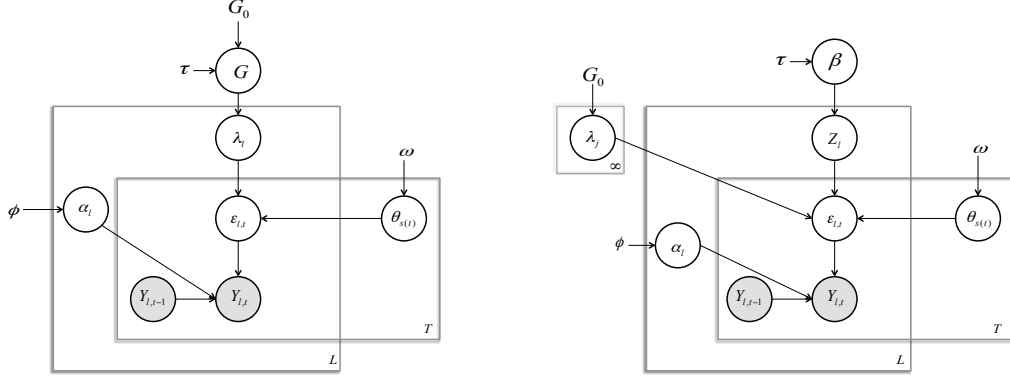


Figure 3: Graphical model of the multivariate dependent PoINAR(1) model. *Left:* Innovations generating from a Dirichlet process mixture model as in Eq. (11). *Right:* An equivalent representation using cluster indicator variables z_1, \dots, z_L as in Eq. (12).

number of clusters is much smaller than the number of observations.

In our model for crime rates, we impose a DP prior on the L tract-specific rates, λ_l . Note that in our application, the number of observations from the DP is equal to the number of tracts, rather than the number of time points. The DP prior thus groups the time series according to their corresponding tract-specific rates into a few clusters. Members of the k^{th} cluster share a common tract rate, ϕ_k . The grouping of the time series into a small number of clusters provides useful shrinkage that pools information across the cluster, thereby yielding more accurate out-of-sample predictions for the multiple time series. When we combine the tract-specific rates and the seasonal effects, we obtain the following generating process for the innovations:

$$\begin{aligned}
\epsilon_{l,t} &\sim \text{Poisson}(\lambda_l \theta_{s(t)}) \quad l = 1, \dots, L \quad t = 1, \dots, T \\
\theta_m &\sim F \quad m = 1, \dots, 12 \\
\lambda_l &\sim G \quad l = 1, \dots, L \\
G &\sim \text{DP}(\tau, G_0).
\end{aligned} \tag{11}$$

For our application, we choose F to be a gamma distribution in Eq. (21).

Figure 3 (left) shows a graphical representation of our dependent multivariate PoINAR(1) process. For details on interpreting such graphical representations, the reader is referred to Jordan (2004). Alternatively, we can use an equivalent representation using the GEM distribution and the membership labels z_1, \dots, z_L (see Figure 3 (right)):

$$\begin{aligned}
\epsilon_{l,t} &\sim \text{Poisson}(\phi_{z_l} \theta_{s(t)}) \quad l = 1, \dots, L \quad t = 1, \dots, T \\
\theta_m &\sim \text{F} \quad m = 1, \dots, 12 \\
z_l &\sim \text{Multinomial}(\beta) \quad l = 1, \dots, L \\
\phi_j &\sim G_0 \quad \beta \sim \text{GEM}(\tau) \quad j = 1, 2, \dots
\end{aligned} \tag{12}$$

3.3 Prior specification

The multivariate PoINAR(1) requires estimation of three main components:

- thinning values $(\alpha_1, \dots, \alpha_L)$, one for each time series.
- monthly seasonal effects, $(\theta_1, \dots, \theta_{12})$.
- rates for each tract, $[\lambda_1, \dots, \lambda_L]$.

The Bayesian framework places prior distributions on each of these three elements. Our priors are both computationally convenient and weakly-informative. For the thinning values and monthly seasonal effects we specify:

$$\begin{aligned}
\alpha_l &\stackrel{\text{iid}}{\sim} \text{Beta}(\eta_1, \eta_2) \quad \text{for } l = 1, \dots, L \\
\theta_m &\stackrel{\text{iid}}{\sim} \text{Gamma}(\xi_1, \xi_2) \quad \text{for } m = 1, \dots, 12.
\end{aligned} \tag{13}$$

We also explored the half-normal distribution as a prior for the seasonal effect, and we found the choice did not reveal any material changes from the results presented in Section 6. The DP requires the specification of the base measure, G_0 , and the concentration parameter, τ .

We choose the base measure to be the $\text{Gamma}(\gamma_1, \gamma_2)$ distribution, which is well suited to our model because not only it is conjugate to the Poisson distribution but it also provides a natural interpretation. In particular, we have a prior belief that weekly rates of violent crime are typically small, but a few tracts have higher rates. Hence, a gamma distribution with shape and scale parameters $\gamma_1 = 1$ and $\gamma_2 = 0.1$ reflects these prior beliefs. For the concentration parameter, we specify $\tau \sim \text{Gamma}(a_\tau, b_\tau)$, as suggested by Escobar and West (1994).

3.4 Relationship to Multivariate Independent AR(1) process

The continuous counterpart to the multivariate PoINAR(1) is the Gaussian multivariate first-order autoregressive process (VAR(1)). This process is composed from L independent AR(1) processes and can be formulated in the following manner:

$$\begin{aligned} \mathbf{Y}_{t+1} &= \boldsymbol{\alpha} \cdot \mathbf{Y}_t + \boldsymbol{\epsilon}_{t+1} \quad t = 1, \dots, T \\ \boldsymbol{\epsilon}_t | \Sigma &\stackrel{\text{iid}}{\sim} N(0, \Sigma) \\ Y_{l,0} | \mu_{l,0}, \sigma_{l,0} &\stackrel{\text{iid}}{\sim} N(\mu_{l,0}, \sigma_{l,0}) \quad l = 1, \dots, L. \end{aligned} \tag{14}$$

where $[\Sigma]_{i,j} = 0$ for $i \neq j$ and $[\Sigma]_{i,i} = \sigma_i^2$. Compare this specification to the multivariate PoINAR(1):

$$\begin{aligned} \mathbf{Y}_{t+1} &= \boldsymbol{\alpha} \circ \mathbf{Y}_t + \boldsymbol{\epsilon}_{t+1} \quad t = 1, \dots, T \\ \boldsymbol{\epsilon}_t | \Lambda_t &\stackrel{\text{iid}}{\sim} [\text{Poisson}(\Lambda_{1,t}), \text{Poisson}(\Lambda_{2,t}), \dots, \text{Poisson}(\Lambda_{L,t})] \\ Y_{l,0} | \Lambda_{l,0} &\stackrel{\text{iid}}{\sim} \text{Poisson}(\Lambda_{l,0}) \quad l = 1, \dots, L. \end{aligned} \tag{15}$$

These two models not only share similar notation, but also possess two common characteristics:

- The distributions of the innovations match the marginal distributions of $Y_{l,t}$. The

PoINAR(1) with diagonal $\boldsymbol{\alpha}$ (having non-negative diagonal entries) has Poisson marginal distributions while the VAR(1) has Gaussian marginals for any $\boldsymbol{\alpha}$. If the parameters defining the processes are chosen carefully, these models can be shown to have a Poisson or Gaussian stationary distribution, respectively.

- The autoregressive parameter $\alpha_{l,l}$ determines the autocorrelation coefficient in both models, $\text{corr}(Y_{l,t+1}, Y_{l,t}) = \alpha_{l,l}$.

These similarities to the continuous VAR(1) make the discrete PoINAR(1) especially attractive and easy to interpret. The VAR(1) process, however, has a single source of variation – the innovations process – while the PoINAR(1) process has two – the binomial thinning and innovations processes. This key difference complicates inference for the PoINAR(1) model, which we address in Section 4.

4 The MCMC Sampler

As previously noted, the PoINAR(1) model is a combination of two underlying processes: the binomial thinning process and the innovations process. Each of these processes has its own parameters: binomial thinning uses the thinning parameters $\{\alpha_l\}$ and the innovations process uses the rates $\{\phi_k\}$ and the seasonal effects $\{\theta_m\}$. For posterior computations within our Bayesian framework, we employ an MCMC sampler. Intuitively, the idea is to sample a posterior latent innovations sequence and then condition on this sequence to sample both the latent DP clustering of census tracts and also the thinning parameters and seasonal effects. In contrast, in the corresponding VAR(1) model there is no need to sample the innovations sequence since they are a deterministic function of the observations and the model parameters. Therefore, one would expect the multivariate PoINAR(1) model to be computationally cumbersome compared to its VAR(1) counterpart. However, our proposed sampler harnesses computational advantages from small observed counts in our crime data

and sufficient statistics implied by the Poisson model. We outline the resulting sampler below. For detailed derivations, see Section A of the Supplementary Material.

1. Sample the innovations, $\boldsymbol{\epsilon} := [\epsilon_1, \dots, \epsilon_L]$ where $\epsilon_l := [\epsilon_{l,1}, \dots, \epsilon_{l,T}]$ is the innovations series for the l^{th} tract. The posterior factors as:

$$P(\boldsymbol{\epsilon} | \mathbf{Y}, \boldsymbol{\alpha}, \boldsymbol{\lambda}, \boldsymbol{\theta}) = \prod_{l=1}^L \prod_{t=2}^T P(\epsilon_{l,t} | Y_{l,t-1}, Y_{l,t}, \alpha_l, \lambda_l, \boldsymbol{\theta}). \quad (16)$$

align Given the observations \mathbf{Y} and the parameters of the multivariate PoINAR process, the innovations can be sampled independently for each tract and each time point. The possible values satisfy $\max\{0, Y_{l,t} - Y_{l,t-1}\} \leq \epsilon_{l,t} \leq Y_{l,t}$ with corresponding probabilities

$$P(\epsilon_{l,t} | Y_{l,t-1}, Y_{l,t}, \alpha_l, \lambda_l, \boldsymbol{\theta}) \propto \frac{1}{\epsilon_{l,t}! (Y_{l,t} - \epsilon_{l,t})! (Y_{l,t-1} - (Y_{l,t} - \epsilon_{l,t}))!} \left(\frac{\lambda_l \theta_{s(t)} (1 - \alpha_l)}{\alpha_l} \right)^{\epsilon_{l,t}}. \quad (17)$$

Although this expression does not define a well-known discrete distribution, it is analytically tractable because of the small counts in the data (i.e., $\max\{0, Y_{l,t} - Y_{l,t-1}\} \leq \epsilon_{l,t} \leq Y_{l,t}$ and $Y_{l,t}$ is assumed to be small). In the crime data for Washington, D.C., $\max Y_{l,t} = 11$. Another important consideration that reduces the computational burden is that certain $\epsilon_{l,t}$ values can be deterministically set from the observations vector \mathbf{Y}_t : if $y_{l,t} = 0$ then $\epsilon_{l,t} = 0$ and if $y_{l,t-1} = 0$ then $\epsilon_{l,t} = y_{l,t}$. Since our crime data has many zero counts, these constraints substantially lower the computational cost of this portion of the sampling. If larger counts are observed, then one can use a Metropolis-Hastings step to sample from this distribution with a Poisson proposal distribution. Importantly, note that if the observed counts are large enough one can apply a stabilizing transformation such as the square root and model the resulting process as a

VAR. This strategy has been shown by Brown et al. (2005) to yield satisfactory results in the univariate case when λ_l is assumed to exceed (roughly) 5.

2. Sample the membership indicator vector, $\mathbf{z} := [z_1, \dots, z_L]$. We harness the DP-induced Chinese restaurant process (CRP) and iteratively sample tract-specific cluster indicators:

$$P(z_l = k | \mathbf{z}_{/l}, \boldsymbol{\epsilon}, \Theta, \gamma_1, \gamma_2, \tau) \propto \begin{cases} \tau p_{l,0} & \text{for } k = K + 1 \\ n_k p_{l,k} & \text{for } k = 1, \dots, K, \end{cases} \quad (18)$$

where $K + 1$ identifies a previously unseen cluster, $\Theta = \sum_{t=1}^T \theta_{s(t)}$ and $\mathbf{z}_{/l}$ is the vector of membership indicators, not including the l^{th} term. The first terms, (τ, n_j) , of Eq. (18) arise from the CRP prior of Eq. (10) and the exchangeability of the process such that each z_l can be treated as the last. The second terms, $(p_{l,0}, p_{l,j})$, correspond to the likelihood of the innovations $\boldsymbol{\epsilon}$ given the cluster assignments $(z_l = k, \mathbf{z}_{/l})$ and seasonal effects Θ , marginalizing the cluster-specific rates ϕ_k . The terms are given by the following negative binomial distributions:

$$\begin{aligned} p_{l,0} &= \frac{\Gamma(S_l + \gamma_1)}{\Gamma(\gamma_1) S_l!} \left(\frac{\gamma_2}{\Theta + \gamma_2} \right)^{\gamma_1} \left(\frac{\Theta}{\Theta + \gamma_2} \right)^{S_l} \\ p_{l,j} &= \frac{\Gamma(S_l + A_j + \gamma_1)}{\Gamma(A_j + \gamma_1) S_l!} \left(1 - \frac{\Theta}{n_j \Theta + \gamma_2} \right)^{A_j + \gamma_1} \left(\frac{\Theta}{n_j \Theta + \gamma_2} \right)^{S_l}, \end{aligned} \quad (19)$$

where $S_l = \sum_{t=1}^T \epsilon_{l,t}$ and $A_j = \sum_{i: z_i=j, i \neq l} S_i$. Note that $p_{l,0}$ and $p_{l,j}$ only rely on sums of the innovations and the sum of seasonal effects. We also highlight that the conditional conjugacy of our formulation allows us to use the collapsed sampler of Eq. (18) for the z_l , marginalizing $\{\phi_k\}$.

3. Sample unique rates, ϕ_k . Although the rates collapse away in sampling the cluster indicators, z_l , they are needed for sampling the innovations sequence (Step 1) and

seasonal effects (Step 3). As such, we instantiate the unique rates as auxiliary variables for these steps, and then discard them. For each currently instantiated cluster, sample ϕ_k as:

$$\phi_k | \boldsymbol{\epsilon}, \mathbf{z}, \Theta, \gamma_1, \gamma_2 \sim \text{Gamma}(B_k + \gamma_1, n_k \Theta + \gamma_2), \quad (20)$$

where $B_k = \sum_{l \in \{v: z_v = k\}} S_l$. Again, we only rely on the sum of the innovations, S_l , to compute the posterior distribution.

4. Sample the seasonal effects vector, $[\theta_1, \dots, \theta_{12}]$. The m^{th} element of this vector can be sampled as:

$$\theta_m | \boldsymbol{\epsilon}, \boldsymbol{\phi}, \xi_1, \xi_2 \sim \text{Gamma} \left(\sum_{l=1}^L \sum_{t: s(t)=m} \epsilon_{l,t} + \xi_1, q_m \sum_{l=1}^L \lambda_l + \xi_2 \right), \quad (21)$$

where q_m counts the number of occurrences of the m^{th} month in the data. Notice that for this step we sum the innovations over tracts rather than time.

5. Sample the vector of thinning parameters, $[\alpha_1, \dots, \alpha_L]$. For tract l ,

$$\alpha_l | \boldsymbol{\epsilon}_l, \mathbf{Y}_l, \eta_1, \eta_2 \sim \text{Beta} \left(\sum_{t=2}^T Y_{l,t} - S_l + \eta_1, \sum_{t=2}^T (Y_{l,t-1} - Y_{l,t}) + S_l + \eta_2 \right), \quad (22)$$

where S_l is defined as in Step 2.

6. Sample the concentration parameter, τ , for the Dirichlet process prior according to Escobar and West (1994).

It is important to note that if the model did not include seasonal effects, then one could simply sample the sum of the innovations, S_l , instead of the vector of innovations, ϵ_l . This would reduce the computational cost of the sampler since Step 1 is the most time consuming.

5 Simulation Examples

In order to demonstrate the performance of our model, we simulate datasets from 9 different multivariate PoINAR(1) processes of Eq. (4). Each dataset has $L = 100$ time series (tracts) with $T = 208$ observations which correspond to 4 years of weekly data samples. We group the multiple time series into four equally sized clusters that each share a common rate. The data sets vary in the choice of:

- The separation between the cluster rates, ϕ_k . We examine an “easy” setting in which the four cluster rates are well separated at 1, 3, 6, 10, a “medium setting” with less distinct rates 0.01, 0.5, 1.2, 2, and a “hard” setting with rates 0.1, 0.2, 0.3, 0.6.
- The thinning values, α_l , which determine the autocorrelation of the individual PoINAR(1) processes. The examples use a common choice for α_l for all tracts in a dataset, choosing from $\alpha_l = 0.1, 0.5, 0.9$.

We evaluate the root mean square error (RMSE) and absolute percentage error (APE) of our MCMC sampler both in- and out-of-sample. These metrics measure the distance between the true population expected value and its corresponding estimate based on the observed $L = 100$ time series. The simulation results show that our model produces accurate out-of-sample forecasts under various configurations. Table 1 presents the RMSE of our Bayesian nonparametric model compared to the RMSE of a simple Poisson process model (SPP) and the conditional least-squares model (CLS). (The Supplementary Material, Section B, details both of these.) The results in Table 1 show that our model outperforms these alternatives. As expected, the larger the separation between the cluster rates, the easier it is for our method to identify the true clusters and yield better estimates for their parameters. Also, higher autocorrelation helps our method produce more accurate estimators.

These simulation results indicate that the sampler finds clusters when they exist. It is also important to demonstrate that the model does not spuriously spawn clusters when the

	Thin=0.1			Thin=0.5			Thin=0.9		
Rates	Easy	Med	Hard	Easy	Med	Hard	Easy	Med	Hard
SPP RMSE	0.477	0.113	0.005	1.674	0.880	0.293	6.128	1.155	0.552
CLS RMSE	0.306	0.080	0.035	0.284	0.114	0.057	0.343	0.118	0.055
BNP RMSE	0.219	0.058	0.026	0.260	0.086	0.045	0.299	0.075	0.043
$E(Y_{.,T+1})$	5.383	1.001	0.317	9.861	1.848	0.591	52.161	9.908	3.0633

Table 1: RMSE of estimates of the conditional mean obtained by the CLS, SPP and our Bayesian nonparametric method. The last row shows the expected (true) conditional expected value.

data are homogeneous. As part of our simulations, we also examined the performance of these methods in the situation in which a single process (cluster) generates all of the time series. The findings are presented in Section C of the Supplementary Material, which also contains a more detailed description of the simulations and results presented in this section. As one would hope, under these conditions we identify a single cluster, further validating our methodology.

6 Violent Crime Data Analysis

In this section we examine both in- and out-of-sample results using the reported counts of violent crimes in Washington, D.C. as described in Section 1. The data consist of $L = 188$ time series (census tracts) with $T = 418$ weeks of counts in 2001 through 2008. We use the first 7 years of data to train our model and the last 52 weeks to evaluate its out-of-sample forecasts. We ran 5 MCMC chains for 5,000 iterations from different initial values, each drawn from the following priors:

$$\begin{aligned}
 \theta_m &\sim \text{Gamma}(1, 1) & \alpha_l &\sim \text{Beta}(1, 1) \\
 \tau &\sim \text{Gamma}(2, 4) & \phi_i &\sim \text{Gamma}(1, 1).
 \end{aligned}
 \tag{23}$$

We performed a sensitivity analysis for the hyperparameters during the simulation stage, but found no significant changes to the results. We discard the first 1000 iterations as burn-in and then thin the remaining 4,000 samples by 50. Therefore, our inference for each

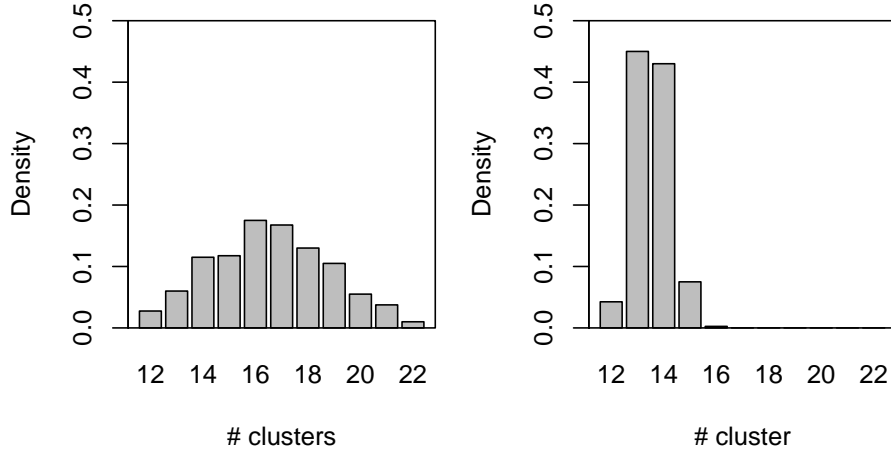


Figure 4: Histograms of the posterior number of clusters for the multivariate dependent PoINAR(1) described in Section 3.2 (left) and the population adjusted multivariate dependent PoINAR(1) model described in Section 7 (right).

parameter of the model is based on the resulting $80 \cdot 5 = 400$ MCMC samples. We use the scale reduction factor (recommended by Gelman and Rubin, 1992) to monitor convergence across the chains.

We begin by looking at the distribution of the number of clusters over the 400 iterations in the left panel of Figure 4. The mode is 17 clusters, which is a substantial reduction from the original $L = 188$ time series. Figure 5 presents a representative cluster assignment along with the posterior rates for this assignment. This cluster assignment is selected as the assignment that has the minimum average Hamming distance across the different iterations (see Fox et al., 2011, for further details.). An interesting phenomenon is that census tracts assigned to the same cluster are frequently spatially separated.

We further examine the posterior means for the rates, λ_l , of the 188 census tracts and their corresponding thinning values, α_l , across the MCMC samples. Figure 6 (left) maps the posterior mean rates for the census tracts in Washington, D.C.. We can see certain regions that exhibit higher rates (e.g., tracts that correspond to a southern portion of the city, a central portion along 16th Street, and an east-central portion along Rhode Island Avenue.)

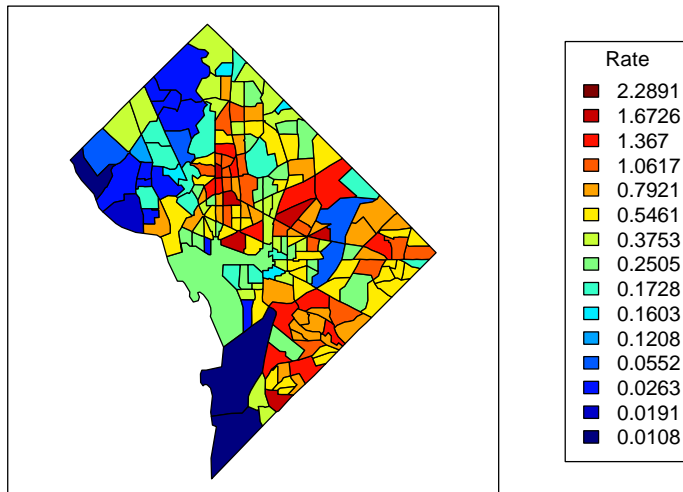


Figure 5: The minimum average Hamming distance cluster assignment along with the corresponding posterior rate values.

The results of Figure 6 are also substantiated by Figure 1 (right). Figure 7 compares, for each census tract, the sample autocorrelation in the counts for each tract with the posterior mean thinning values. The sample autocorrelation is calculated using the classical first order autocorrelation estimator for each time series separately (without adjusting for seasonality). As previously explained, the thinning values in our model determine the autocorrelation for each INAR(1) time series. The comparison shows that the raw data autocorrelations vary on a wider range of values than their corresponding posterior mean values and some of these raw autocorrelations are slightly negative. There are two reasons that can account for the differences between the two:

1. Our model only allows the thinning value to range between $[0, 1]$ and therefore cannot account for negative autocorrelation. We believe that the (small) negative raw autocorrelations are probably due to noise variation and therefore we are less concerned about this phenomenon. The standard error of an estimated first-order autocorrelation for white noise is approximately $1/\sqrt{T} = 1/\sqrt{418} \approx 0.05$; hence the bulk of raw autocorrelations are within about 2 standard errors of zero.

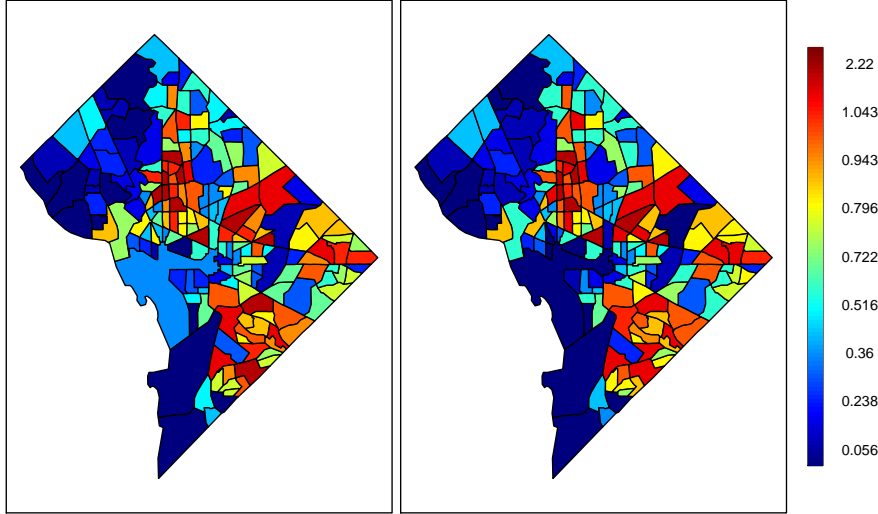


Figure 6: Map of posterior mean rates, λ_l , sampled from the multivariate dependent PoINAR(1) model described in Section 3.2 (left) and the population adjusted multivariate dependent PoINAR(1) model described in Section 7 (right).

2. The posterior mean thinning values are adjusted for seasonal effects, whereas the raw autocorrelations are not. The values would be smaller in magnitude after adjusting for the seasonality, as our results suggest.

For the out-of-sample evaluation we compare our MCMC method to the CLS and SPP. For both the CLS and our method, we use the estimated one-week-ahead conditional mean as the predictor for the crime counts in each tract:

$$\hat{y}_{l,T+1} = \alpha_l y_{l,T} + \lambda_l \theta_{s(T+1)}. \quad (24)$$

For CLS, we simply plug-in the estimates of α_l , λ_l and θ_m for each tract. For our method, we compute an MCMC-based estimate by evaluating Eq. (24) for each of the 400 MCMC iterations and use the average of these as the final predicted value (see Section C.2 of the Supplementary Material for further details). For the SPP, we average the past values as the predictor.

We predict the one-week-ahead number of crimes in each tract for the first week of each

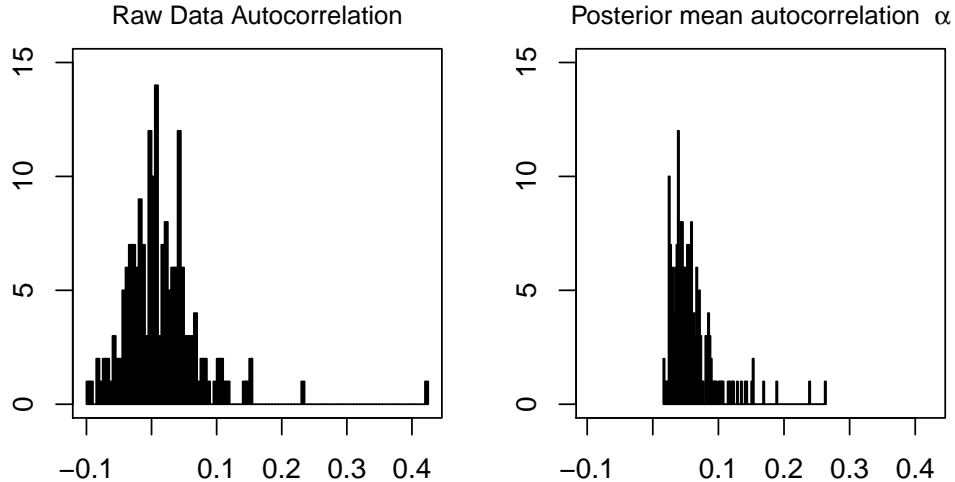


Figure 7: Histogram of raw data autocorrelations (left) and posterior mean autocorrelations α_l (right).

month during 2008. Table 2 shows the one-week-ahead predicted mean RMSE and corresponding standard errors, conditional on the last observed value. The results indicate that when the last observed count is one of the most frequent values (0,1,2), our method produces lower RMSE. For the less frequent, higher counts (3,4), the performances of all of the methods are (statistically) equivalent. This behavior is to be expected since our method shrinks the estimators toward the mean and therefore should perform better for lower, more frequent counts and worse in the more rare cases of high counts. A summary of the average one-week-ahead bias is presented in Section F of the Supplementary Material. In general, our method produces the smallest bias, but the differences between the methods are not significant except when the last observed count is zero.

The one-step-ahead conditional mean value is the best linear unbiased estimator under quadratic loss. Since the CLS method minimizes the observed squared error, it is only natural to evaluate all three methods using the same loss function. Alternatively, Berk (2008) proposed a quantile loss function that reflects the sensitivity of the police department to forecasting errors. Under a v -quantile loss function, the predictor is just the predictive distribution's v quantile. Using our method, one can easily sample from the following one-

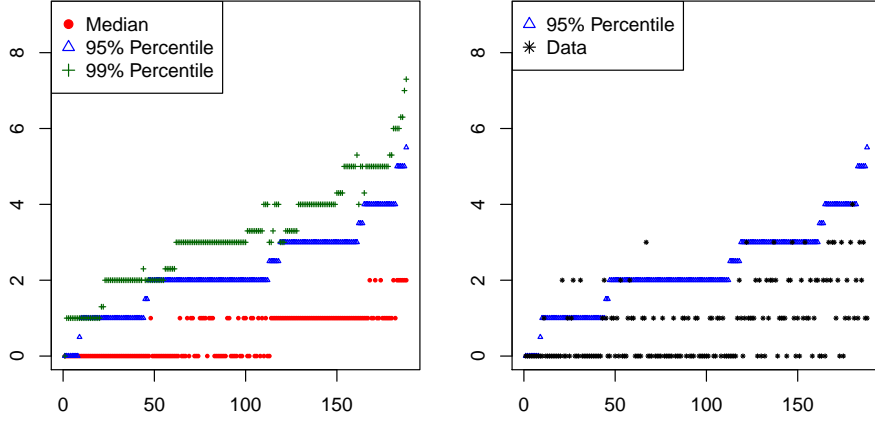


Figure 8: The predictive posterior distribution for each of the 188 tracts. The red dots correspond to the median predicted number of violent crimes for each tract. The blue triangles and green crosses correspond to the 95% and 99% percentiles of the predictive posterior distribution, respectively. The black stars corresponds to the test-set actual observed value of crimes.

step-ahead predictive posterior distribution and evaluate any desired quantile:

$$P(Y_{l,t+1} = y_{l,t+1} | Y_{l,t} = y_{l,t}, \alpha_l^{(m)}, \boldsymbol{\theta}^{(m)}, \lambda_l^{(m)}) = \sum_{r=0}^{\infty} \binom{y_{l,t}-1}{y_{l,t}-r} (\alpha_l^{(m)})^{y_{l,t}-r} (1 - \alpha_l^{(m)})^{y_{l,t-1}-(y_{l,t}-r)} \frac{e^{-\phi_l^{(m)} \theta_{s(t+1)}^{(m)}} (\phi_l^{(m)} \theta_{s(t+1)}^{(m)})^r}{r!}, \quad (25)$$

where $\lambda_l^{(m)} = \phi_{z_l^{(m)}}^{(m)}$, $\boldsymbol{\theta}^{(m)}$ and $\alpha_l^{(m)}$ are the rate, seasonal component and thinning value estimated during the m^{th} iteration of the MCMC sampler. Figure 8 shows the 95% and 99% quantiles for each of the 188 tracts and the corresponding one-step-ahead true value, $y_{l,T+1}$. The quantiles may also be used to provide prediction intervals for each tract. A police department can use these intervals along with the point estimate to distinguish between an unusual surge in crimes which requires allocation of more resources, and a random rise in crimes, which would not benefit from an intervention.

$y_{\cdot,T}$	0	1	2	3	4	Overall
SPP RMSE	0.8373 (0.034)	0.966 (0.0311)	1.1829 (0.0453)	1.4722 (0.088)	1.4252 (0.1631)	0.970 (0.0167)
CLS RMSE	0.7729 (0.0245)	0.9501 (0.0430)	1.0605 (0.0660)	1.1370 (0.0982)	1.3258 (0.1991)	0.9235 (0.0368)
Dependent PoINAR RMSE	0.7222 (0.0135)	0.9172 (0.0172)	1.009 (0.4336)	1.0225 (0.0862)	1.1600 (0.1782)	0.72168 (0.0016)
Frequency	0.5900	0.2340	0.1160	0.0400	0.0200	1

Table 2: One-step-ahead average RMSE as a function of the last observed value of $y_{\cdot,T}$. We also provide the standard errors associated with the average RMSE.

7 Covariates Adjusted Dependent PoINAR(1)

Previous research has shown that the tracts of crime are associated with demographic covariates, and we have several ways to incorporate such features into our Bayesian model. For example, Blei and Frazier (2010) incorporate covariates directly into the clustering mechanism. This approach might improve the accuracy of forecasts, but it would provide less in the way of interpretation, such as how the various covariates associate with crime rates. Instead, we take a more direct approach that offers the advantages of clustering as well as interpretation. We model the tract-specific rate λ_l as a linear function of covariates and cluster the coefficients of the equation. The clusters of coefficients may provide further insight into the relationships between crime and demographic characteristics.

7.1 Adjusting for population

The main goal of this section is to demonstrate how to add covariates to our model and to explore the benefits of doing so. To this end, we look at the population sizes in each of the census tracts as a possible explanatory variable.

Let X_l denote the population of the l^{th} census tract. (We obtain the populations from the 2000 census. Section D of the Supplementary Material shows a map of the population density in Washington, D.C..) To incorporate population into our model, we redefine the tract-specific rate as a linear function of population, i.e. $\lambda_l = X_l \psi_l$, where ψ_l is the number

of violent crimes per person in the l^{th} tract. We then place a DP prior directly on the rate per person parameter, ψ_l , yielding the following model:

$$\begin{aligned}
\epsilon_{l,t} &\sim \text{Poisson}(X_l \psi_l \theta_{s(t)}) \quad l = 1, \dots, L \quad t = 1, \dots, T \\
\theta_m &\sim \text{F}(\omega) \quad m = 1, \dots, 12 \\
\psi_l &\sim \text{G} \quad l = 1, \dots, L \\
\text{G} &\sim \text{DP}(\tau, G_0).
\end{aligned} \tag{26}$$

It is straightforward to adjust the MCMC sampler described in Section 4 to incorporate the population covariate, X_l . We change the base measure G_0 to Gamma(0.5,0.5) to reflect the adjustment for population sizes while remaining weakly informative. After these simple modifications, we run the sampler in the manner previously described in Section 4.

7.2 Analysis of results

Using the covariate-adjusted PoINAR(1) of Section 7.1, we again analyze the counts of violent crimes in Washington. As in Section 6, we begin by showing the posterior distribution of the number of clusters over the 400 MCMC iterations (again taken from 5 chains, each run for 5,000 iterations). Figure 4 (right) indicates that the distribution is much narrower when we adjust for the population density, and has a mode of 14 clusters. This suggests that population can account for a significant amount of the spatial heterogeneity in crime. Figure 9 maps the posterior means of the crime rate per person, ψ_l . This map highlights three main features:

1. The center of Washington, D.C. has a high count of violent crimes per person.
2. The northwest portion of the city has very few crimes per person.
3. The city has three hot-spots: in the center of the city and in the eastern and southwestern portions of the city.

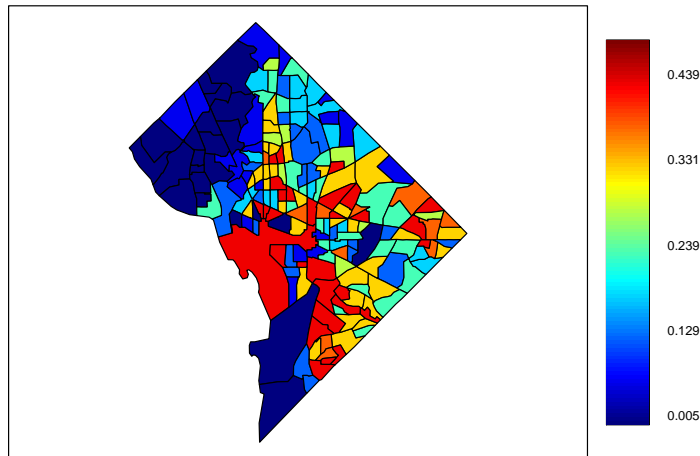


Figure 9: Map of the posterior mean values for crime rates per person, ψ_i .

These insights, also highlighted by Cahill and Roman (2010), differ from the conclusions one would make by simply looking at the mean values as shown in Figure 1 or from our previous analysis. The results emphasize tracts which exhibit high crime rates per person as opposed to high crime counts and can help police make future planning decisions, such as where to place a new station. These outcomes, important as they may be, are merely a byproduct of our estimation method. The more interesting research question is whether the population covariate can improve the prediction abilities when compared to the unadjusted model.

We performed a one-week-ahead forecast for the last week in the series using both the unadjusted model of Section 3.2 and the adjusted model accounting for population. The overall RMSE of the unadjusted model was 0.9663 whereas the adjusted model was 0.9713. These results suggest that adding the population of the tract to the model does not necessarily improve predictive accuracy. However, a more extensive analysis would be needed to confidently settle such issues. Although adding the population of the tract to the model may not improve predictive accuracy, adding the covariate seems to provide a useful benefit in that the revised model reveals a more interpretable grouping of the time series. Of course, there are many other covariates that one could consider, for example measures of poverty, housing characteristics, etc.

8 Discussion

In this paper we have presented a method of forecasting multiple correlated low-count time series building on the univariate PoINAR framework. The model induces correlation between the different time series through two sources: an overall temporal seasonal effect and a clustering on individual rate parameters. The latter clustering is induced by a Dirichlet process, which encourages sparse representations in terms of a small number of clusters. The grouping of the different rates allows our model to borrow strength across the different time series, shrinking the estimators to provide better out-of-sample forecasts.

Our model assumes that there is some underlying clustering assignment of the multiple time series. Moreover, once these clusters are identified, they remain fixed throughout time. One can relax this assumption and allow for temporally evolving cluster assignments. There are a few ways to create such a mechanism, for example we might impose dependent Dirichlet process priors, such as those examined by Taddy (2010).

Finally, although our focus here is on counts of violent crimes, this model is broadly applicable to many low-count spatio-temporal data sets, including the number of insurance claims across the U.S., earthquakes across the globe (Boudreault and Charpentier, 2011), wildfires across counties (Xu, 2011), and so forth.

References

- A. Alzaid and M. Al-Osh. First order integer valued autoregressive process: Distributional and regression properties. *Statistica Neerlandica*, 42(1):53–61, 1988.
- R. Berk. Forecasting methods in crime and justice. *Annual Review of Law and Social Science*, 4(1):219–238, 2008.
- D. M. Blei and P. I. Frazier. Distance dependent Chinese restaurant processes. *Journal of Machine Learning Research*, 12:2461–2488, 2010.

- M. Boudreault and A. Charpentier. Multivariate integer-valued autoregressive models applied to earthquake counts. *eprint arXiv:1112.0929*, December 2011. <http://adsabs.harvard.edu/abs/2011arXiv1112.0929B>.
- K. Brännäs. *Estimation and testing in integer-valued AR(1) models*. University of Umeå, 1993.
- L. D. Brown, N. Gans, A. Mandelbaum, A. Sakov, H. Shen, S. Zeltyna, and L. Zhao. Statistical analysis of a telephone call center: A queueing science perspective. *Statistical Science (Special Issue on Bayesian Statistics)*, 100:36–50, 2005.
- M. Cahill and J. K. Roman. Small number of blocks account for lots of crime in D.C., November 2010. http://www.dccrimepolicy.org/Briefs/images/DCPIBrief_CrimeByBlockFINAL_2.pdf.
- R. M. Dorazio, B. Mukherjee, L. Zhang, M. Ghosh, H. L. Jelks, and F. Jordan. Modeling unobserved sources of heterogeneity in animal abundance using a Dirichlet process prior. *Biometrics*, 64(2):635–644, 2008.
- M. D. Escobar and M. West. Bayesian density estimation and inference using mixtures. *Journal of the American Statistical Association*, 90:577–588, 1994.
- E. B. Fox, E. B. Sudderth, M. I. Jordan, and A. S. Willsky. Bayesian nonparametric methods for learning Markov switching processes. *IEEE Signal Processing Magazine*, 27(6):43–54, 2010.
- E. B. Fox, E. B. Sudderth, M. I. Jordan, and A. S. Willsky. A sticky HDP-HMM with application to speaker diarization. *The Annals of Applied Statistics*, 5(2):1020–1056, 2011.
- A. Gelman and D. Rubin. Inference from iterative simulation using multiple sequences. *Statistical Science*, 7(4):457–472, 1992.
- M. I. Jordan. Graphical models. *Statistical Science (Special Issue on Bayesian Statistics)*, 19:140–155, 2004.
- D. McDowall, C. Loftin, and M. Pate. Seasonal cycles in crime, and their variability. *Journal*

- of Quantitative Criminology*, 28(3):389–410, 2012.
- E. McKenzie. Discrete variate time series. *Simulation*, 21:1–34, 2000.
- X. Pedeli and D. Karliss. A bivariate INAR(1) process with application. *Statistical Modeling*, 11(4):325–349, 2011.
- J. Pitman. *Combinatorial stochastic processes*. Springer-Verlag, 2006. Lecture Notes for St. Flour Summer School.
- J. Sethuraman. A constructive definition of Dirichlet priors. *Statistica Sinica*, 4(2):639–650, 1994.
- F. W. Steutel and K. Van Harn. Discrete operator-self decomposability and queueing networks. *Communications in Statistics. Stochastic Models*, 2(2):161–169, 1986.
- M. A. Taddy. Autoregressive mixture models for dynamic spatial Poisson processes: Application to tracking intensity of violent crime. *Journal of the American Statistical Association*, 105(492):1403–1417, 2010.
- Y. W. Teh. Dirichlet process. In *Encyclopedia of Machine Learning*, pages 280–287. Springer, 2011.
- Y. W. Teh, M. I. Jordan, M. J. Beal, and D. M. Blei. Hierarchical Dirichlet processes. *Journal of the American Statistical Association*, 101(476):1566–1581, 2006.
- R. L. Wolpert and L. D. Brown. Stationary infinitely-divisible Markov processes with non-negative integer values. April 2011. <http://www-stat.wharton.upenn.edu/~lbrown/Papers/2011d%20Stationary%20Infinitely-Divisible%20Markov%20Processes%20with%20Non-negative%20Integer%20Values.pdf>.
- H. Xu. Point process modeling of wildfire hazard in Los Angeles County, California. *The Annals of Applied Statistics*, 5(2):684–704, 2011.

SUPPLEMENTARY MATERIAL:

Spatio-temporal Low Count Processes with Application to Violent Crime Events

This supplementary material provides further details on our MCMC sampler in Section A and the baseline models to which we compare in Section B. In Section C, we elaborate upon the simulation studies outlined in the main paper. Finally, in Sections D- F, we provide additional details on our Washington, D.C. crime data and results.

A MCMC sampler derivation

In this section, we detail the derivation of the sampling steps presented in Section 4 of the main paper. We first introduce the following notation:

- $S_i = \sum_{t=1}^T \epsilon_{i,t}$
- $\mathbf{S} = [S_1, \dots, S_N]$
- $\mathbf{S}_{-i} = [S_1, \dots, S_{i-1}, S_{i+1}, \dots, S_N]$
- $z_{-i} = [z_1, z_2, \dots, z_{i-1}, z_{i+1}, \dots, z_N]$
- $\Theta = \sum_{t=1}^T \theta_{s(t)}$

Step 1 – Sampling the innovations vectors In Step 1 of the MCMC sampler (Section 4) we motivate the sampling of the innovation vector. We have shown in Eq. (16) that conditional on the data and other model parameters, the innovations are independent of each other and we only need to sample $\epsilon_{i,t}$ when both the current observed value, $y_{i,t}$, and the previous observed value, $y_{i,t-1}$, have positive values. The values of $\epsilon_{i,t}$ in this case will range between $\max\{0, y_{i,t} - y_{i,t-1}\} \leq \epsilon_{i,t} \leq y_{i,t}$. Otherwise, $\epsilon_{i,t}$ is set deterministically. The

distribution of a single innovation, $\epsilon_{i,t}$ is a :

$$\begin{aligned}
P(\epsilon_{i,t}|y_{i,t-1}, y_{i,t}, \alpha_i, \lambda'_i, \boldsymbol{\theta}) &\propto P(y_{i,t}|\epsilon_{i,t}, y_{i,t-1}, \alpha_i)P(\epsilon_{i,t}|\lambda'_i, \boldsymbol{\theta}) \\
&= \binom{y_{i,t-1}}{y_{i,t} - \epsilon_{i,t}} \alpha_i^{(y_{i,t} - \epsilon_{i,t})} (1 - \alpha_i)^{(y_{i,t-1} - (y_{i,t} - \epsilon_{i,t}))} \frac{e^{-\lambda_{z_i} \theta_{s(t)}} \cdot (\lambda_{z_i} \cdot \theta_{s(t)})^{\epsilon_{i,t}}}{\epsilon_{i,t}!} \\
&\propto \frac{1}{\epsilon_{i,t}!(y_{i,t} - \epsilon_{i,t})!(y_{i,t-1} - (y_{i,t} - \epsilon_{i,t}))!} \left(\frac{\lambda_{z_i} \theta_{s(t)} (1 - \alpha_i)}{\alpha_i} \right)^{\epsilon_{i,t}} \\
&= \frac{1}{C_i} \frac{1}{\epsilon_{i,t}!(y_{i,t} - \epsilon_{i,t})!(y_{i,t-1} - (y_{i,t} - \epsilon_{i,t}))!} \left(\frac{\lambda_{z_i} \theta_{s(t)} (1 - \alpha_i)}{\alpha_i} \right)^{\epsilon_{i,t}}
\end{aligned}$$

We can calculate the normalization constant C_i by summing over all the possible values of $\epsilon_{i,t}$ for a given set of values of $y_{i,t}$ and $y_{i,t-1}$.

Step 2 – Sampling the membership indicator In the following equations we construct the posterior distribution for the membership indicator variable:

$$P(z_i = j | \mathbf{z}_{-i}, \mathbf{S}, \boldsymbol{\theta}) \propto P(S_i | S_l \quad l \in \{v : z_v = j, v \neq i\}, \boldsymbol{\theta}) \cdot P(z_i = j | z_l \quad l \in \{v : z_v = j, v \neq i\}).$$

It is straightforward to show that the above distribution has the following form:

$$P(z_i = k | \mathbf{z}_{-i}, \mathbf{S}, \boldsymbol{\theta}) \propto \begin{cases} \alpha \cdot p_{i,0} & \text{for } k = K + 1 \\ n_k \cdot p_{i,k} & \text{for } k = 1, \dots, K, \end{cases}$$

where $p_{i,0}, p_{i,1}, \dots, p_{i,K}$ take on values from the following negative binomial distributions:

$$\begin{aligned}
p_{i,0} &= \frac{\Gamma(S_i + \gamma_1)}{\Gamma(\gamma_1) S_i!} \left(\frac{\gamma_2}{\Theta + \gamma_2} \right)^a \left(\frac{\Theta}{\Theta + \gamma_2} \right)^{S_i} \\
p_{i,j} &= \frac{\Gamma(S_i + A_j + \gamma_1)}{\Gamma(A_j + \gamma_1) S_i!} \left(1 - \frac{\Theta}{n_j \cdot \Theta + \gamma_2} \right)^{A_j + \gamma_1} \left(\frac{\Theta}{n_j \cdot \Theta + \gamma_2} \right)^{S_i} \quad j = 1, \dots, K,
\end{aligned}$$

and $n_j = \sum_{i=1}^L \mathbb{I}_{z_i=j}$ and $A_j = \sum_{l:z_l=j, l \neq i} S_l$. This distribution corresponds to the posterior distribution shown in Step 2 of the MCMC sampler (Section 4).

Step 3 – Sampling the unique rate vector Since we use a gamma distribution as the DP base measure, the resulting conditional posterior distribution for the unique cluster-specific rates is as follows:

$$\begin{aligned} P(\phi_k | \mathbf{z}, \mathbf{S}, \boldsymbol{\theta}, \gamma_1, \gamma_2) &\propto P(\mathbf{S}_l, \quad l \in \{v : z_v = k\} | \phi_k, \boldsymbol{\theta}, \gamma_1, \gamma_2) \cdot P(\phi_k | \gamma_1, \gamma_2) \\ &\propto \phi_k^{B_k + \gamma_1 - 1} e^{-\phi_k \cdot (n_k \cdot \Theta + \gamma_2)} \end{aligned}$$

This has the form of a gamma distribution with parameters $B_k + \gamma_1$ and $n_k \cdot \Theta + \gamma_2$ where $B_k = \sum_{l \in \{v: z_v=k\}} S_l$ which is the distribution described in Step 3 of the MCMC sampler (Section 4).

Step 4 – Sampling the seasonal effect Let $R_t = \sum_{i=1}^L \epsilon_{i,t}$, then the conditional posterior distribution for the seasonal effect is:

$$\begin{aligned} P(\theta_j | \boldsymbol{\lambda}, \mathbf{z}, \boldsymbol{\epsilon}, \xi_1, \xi_2) &\propto P(\boldsymbol{\epsilon}_t, \quad t \in \{t : s(t) = j\} | \boldsymbol{\lambda}, \xi_1, \xi_2) \cdot P(\theta_j | \xi_1, \xi_2) \\ &\propto \theta_j^{\sum_{t:s(t)=j} R_t + \xi_1 - 1} e^{-\theta_j \cdot (m_j \cdot \sum_{l=1}^L \lambda'_l + \xi_2)} \end{aligned}$$

As previously described in Step 4 of the MCMC sampler (Section 4), this is a gamma distribution with parameters $\sum_{t:s(t)=j} R_t + \xi_1$ and $m_j \cdot \sum_{l=1}^L \lambda'_l + \xi_2$ where $m_j = |\{t : s(t) = j\}|$.

Step 5 – Sampling the thinning value The prior distribution for the thinning value α_i is a beta distribution, resulting in the conditional posterior distribution:

$$P(\alpha_i | \mathbf{y}, \boldsymbol{\epsilon}, \eta_1, \eta_2) \propto \alpha^{\sum_{t=2}^T (y_{i,t} - \epsilon_{i,t}) + \eta_1 - 1} \cdot (1 - \alpha)^{\sum_{t=2}^T (y_{i,t-1} - (y_{i,t} - \epsilon_{i,t})) + \eta_2 - 1}$$

As previously described in Step 5 of the MCMC sampler (Section 4), this is a beta distribution with parameters $\sum_{t=2}^T y_{i,t} - S_i + \eta_1$ and $\sum_{t=2}^T (y_{i,t-1} - y_{i,t}) + S_i + \eta_2$.

Step 6 – Sampling the concentration parameter

We follow Escobar and West (1994) and use a gamma distribution prior for the concentration parameter, τ . This stage requires first sampling an auxiliary variable κ which is then used to sample τ :

1. Sample $\kappa \sim \text{Beta}(\tau + 1, L)$.
2. Sample τ as the following mixture of two gammas:

$$\begin{aligned} \tau | \kappa, K &\sim \pi \text{Gamma}(a_\tau + K, b_\tau - \log(\kappa)) \\ &+ (1 - \pi) \text{Gamma}(a_\tau + K - 1, b_\tau - \log(\kappa)), \end{aligned}$$

with weight π defined by $\pi / (1 - \pi) = (a_\tau + K - 1) / (L \cdot [b_\tau - \log(\kappa)])$ where K is the number of unique clusters.

B Conditional least squares model

The PoINAR(1) model can be described in the following manner:

$$y_{t+1} = \alpha \circ y_t + \epsilon_{t+1} \quad t = 1, \dots, T - 1 \tag{27}$$

$$\epsilon_t \sim \text{Pois}(\lambda \cdot \theta_{s(t)}) \tag{28}$$

The one-step-ahead conditional expected value for y_{t+1} is:

$$\hat{y}_{t+1} = \alpha \cdot y_t + \lambda \cdot \theta_{s(t)} \quad (29)$$

The conditional least squares methods estimates this model's parameters by solving the following equation

$$\min_{\lambda, \alpha, \theta_1, \dots, \theta_{12}} \sum_{t=2}^T (y_t - \hat{y}_t)^2 = \min_{\lambda, \alpha, \theta_1, \dots, \theta_{12}} \sum_{t=2}^T (y_t - \alpha \cdot y_t + \lambda \cdot \theta_{s(t)})^2 \quad \text{s.t.} \quad \sum_{s=1}^{12} \theta_s = 1. \quad (30)$$

This is a nonlinear convex optimization problem. The Lagrangian method yields the following conditions:

$$\alpha = \frac{\sum_{t=2}^T y_t \cdot y_{t-1}}{\sum_{t=2}^T y_{t-1}^2} - \lambda \cdot \frac{\sum_{t=2}^T \theta_{s(t)} y_{t-1}}{\sum_{t=2}^T y_{t-1}^2} \quad (31)$$

$$\lambda = \frac{\left(\sum_{t=2}^T y_{t-1}^2\right) \cdot \left(\sum_{t=2}^T y_t \cdot \theta_{s(t)}\right) - \left(\sum_{t=2}^T y_t \cdot y_{t-1}\right) \left(\sum_{t=2}^T y_{t-1} \theta_{s(t)}\right)}{\left(\sum_{t=2}^T y_{t-1}^2\right) \cdot \left(\sum_{t=2}^T \theta_{s(t)}^2\right) - \left(\sum_{t=2}^T y_{t-1} \cdot \theta_{s(t)}\right)^2} \quad (32)$$

$$\theta_i = \frac{2 \cdot \lambda \sum_{t:s(t)=i} (y_t - \alpha \cdot y_{t-1}) - C}{2\lambda^2 \cdot n_i} \quad i = 1, \dots, 12 \quad (33)$$

$$C = \frac{2 \cdot \lambda}{\sum_{i=1}^{12} \frac{1}{n_i}} \left(\sum_{i=1}^{12} \left[\frac{\sum_{t:s(t)=i} (y_t - \alpha \cdot y_{t-1})}{n_i} \right] - \lambda \right) \quad (34)$$

Starting from a set of initial values, we can iterate between these equations and converge to a solution. The convergence is met within a few cycles.

C Simulation study

To assess the performance of our model, we simulate 9 different datasets from our multivariate PoINAR(1) process. Each dataset has $L = 100$ time series (locations) with $T = 208$ observations. The multiple time series are grouped into four equally sized clusters defined by a shared rate value, ϕ_k . The different data sets vary in the levels of separation between the

cluster rates and the time series autocorrelation values, α_l . In this section, we evaluate the performance of our methods both in- and out-of-sample. The results show that our model can reasonably recover the ground-truth clusterings and also produce accurate out-of-sample forecasts under various settings. Our model also outperforms the conditional least-squares model (CLS), which is detailed in Section B. One reasonable explanation for these results is that the CLS model does not allow for sharing of information between the time series and therefore is more prone to noise variation.

C.1 Simulations settings

We have two main factors that we configure in each of the simulated data sets:

- The clusters’ assigned rate values ϕ_k . We examine an “easy” setting in which the four cluster rate values are 1, 3, 6, 10, a “medium setting” with values 0.01, 0.5, 1.2, 2 and a “hard” setting with values 0.1, 0.2, 0.3, 0.6. The rates values are well separated in the easy setting and becomes harder to distinguish as we move to the hard setting.
- The thinning value α_l , which directly relates to the autocorrelation values of the individual PoINAR(1) processes. We use three different thinning values shared between all locations: 0.1, 0.5, 0.9.

Figure 10 illustrates examples of the simulated data for the three different rate scenarios using a thinning value of 0.3. In the “easy” setting, the tract means fall into four clear clusters. In the “hard” setting, it is much more difficult to distinguish between the four clusters solely based on the tract means. Furthermore, we can see that as the thinning value grows the tract means become larger and consequently it is easier to identify the clusters.

C.2 Simulation results

Although we are primarily interested in the out-of-sample performance of our method, there are still two important measures that are useful to examine in-sample: (i) How many

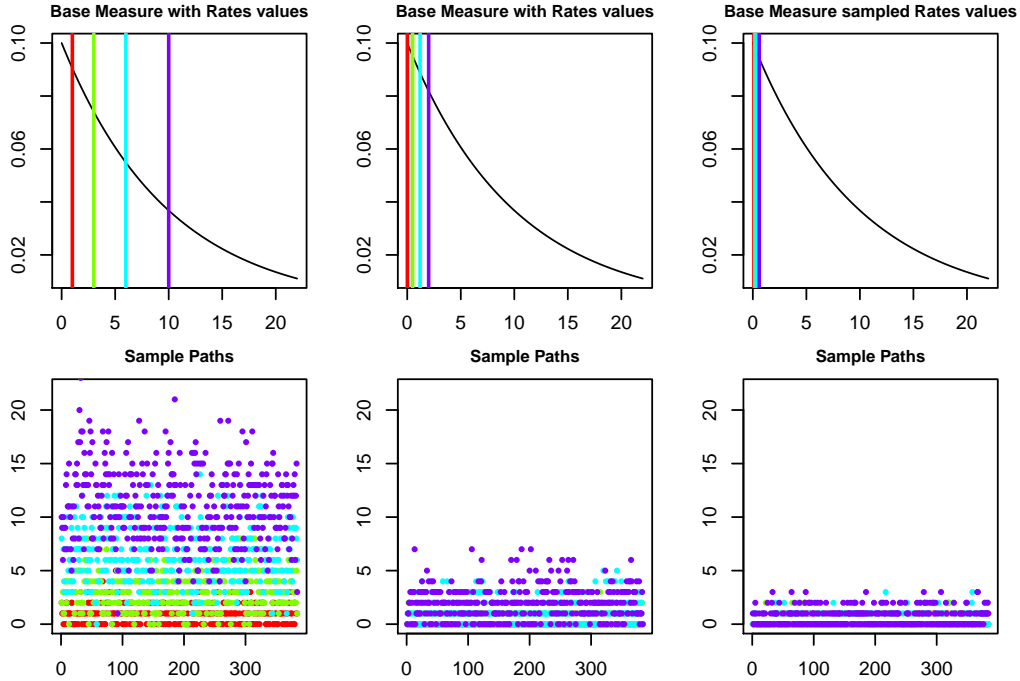


Figure 10: The top panel shows the rates values for the four different clusters, along with the prior distribution for the rates. The lower panel shows an example of 4 overlaid simulated time series. Each time series corresponds to a different cluster and is colored accordingly.

clusters does our method recover? (ii) How close is the recovered clustering assignment to the true assignment? By finding accurate clusterings, our method can borrow information across the multiple time series yielding more accurate out-of-sample predictions.

We run our sampler for 1000 iterations for each of the 9 settings. Figure 11 displays histograms for the number of inferred clusters for each of the scenarios plotted in Figure 10. Figure 11 also shows the Hamming distances between the estimated and true clustering assignment labels. The distances are calculated by first choosing the optimal mapping of indices maximizing overlap between the true and estimated labels assignment sequences. As seen, the modal number of clusters is four in all of the three settings and, as expected, the method recovers the true clustering assignment more accurately for the easy setting than for the hard one. However, even for the hard setting, the Hamming distance errors are usually less than 10% indicating that most time series are correctly clustered. Although we only

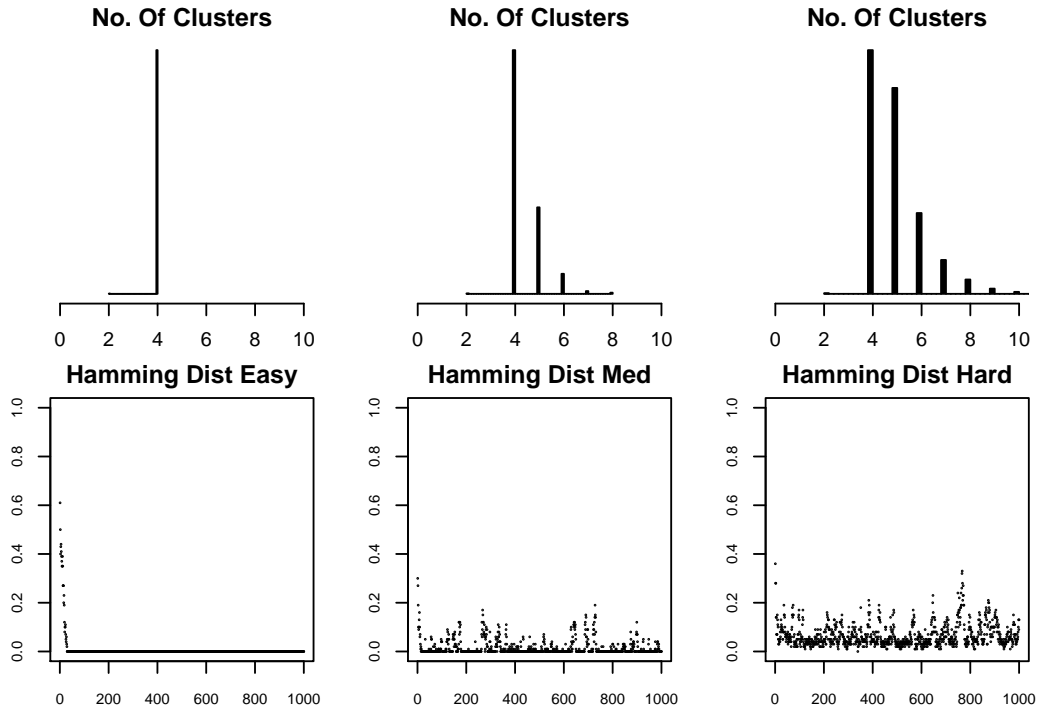


Figure 11: In-sample simulations results. The top panel displays the histogram for the number of clusters over the 1000 iterations. The bottom panel shows the Hamming distance errors between the estimated and true cluster assignments versus MCMC iteration.

display the in-sample analysis for these three settings, these results generally hold for all 9 settings.

An interesting question is whether the methodology finds clustering structure when in fact all the time series belong to the same cluster. To examine this, we simulate a data set that has all of the time series grouped into a single cluster. Figure 12 shows the data and the results for the corresponding MCMC sampler. The model predominantly prefers to group all of the time series together, as we would hope in such a case.

In order to evaluate our model's estimation performance, we compare the estimated one-step-ahead conditional expectation of the PoINAR(1) versus its corresponding true (simulated) population value. Brännäs (1993) showed that the h -step-ahead conditional expecta-

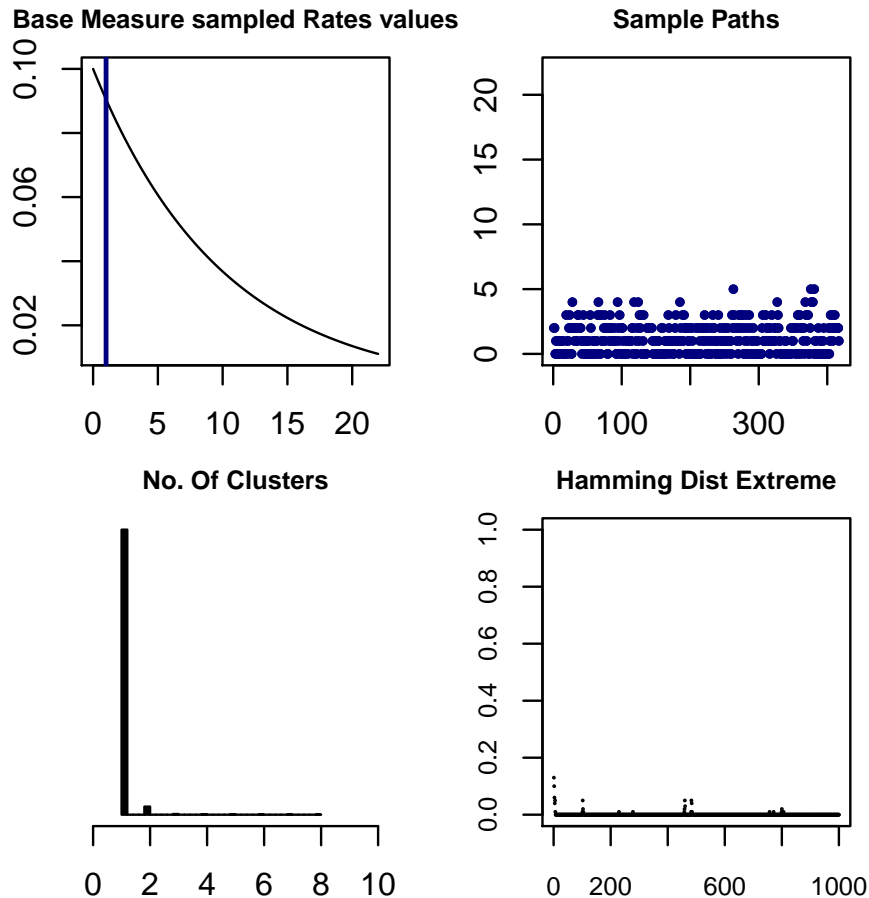


Figure 12: Simulation results for a case where there is a single cluster. The top panels display the single cluster rate value and an example of one of the time series' count data. The bottom panels display the histogram of the number of clusters our method finds and the corresponding Hamming distance errors versus MCMC iteration.

tion of the PoINAR(1) model is:

$$\begin{aligned}
\hat{y}_{T+h} &= \mathbb{E}(y_{T+h}|y_1, \dots, y_T) \\
&= \mathbb{E}(\alpha^h \circ y_T + \sum_{j=1}^h \alpha^{h-j} \circ \epsilon_{T+j}|y_T) \\
&= \alpha^h \cdot y_T + \lambda \sum_{j=1}^h \alpha^{h-j} \cdot \theta_{s(T+j)}.
\end{aligned} \tag{35}$$

To use this predictor for our multivariate PoINAR(1) process, we need to produce estimators

for the rates value, $\boldsymbol{\lambda}$, the seasonal effects values, $\boldsymbol{\theta}_s$, and the thinning value, $\boldsymbol{\alpha}$, for the L time series. To this end, we run the MCMC sampler for $m = 1000$ iterations and discard the first 100 of them as burn-in. We then thin every 5th iteration which leaves us with 180 iterations from which to infer the parameters in our model. The one-step-ahead conditional expected value for the m^{th} iteration is:

$$\hat{y}_{T+1} | \lambda_i^{(m)}, \alpha_i^{(m)}, \boldsymbol{\theta}^{(m)} = \alpha_i^{(m)} \cdot y_T + \lambda_i^{(m)} \cdot \theta_{i,s(T+j)}^{(m)} \quad (36)$$

For each time series (location), we now have samples from the posterior distribution of the conditional expected value which we average to produce the corresponding estimated value. We compare the performance of our method with two benchmark methods: the conditional least-squares (CLS) method and a simple Poisson process (SPP). Since the CLS method models the PoINAR(1) process for each time series separately, we estimate its parameters correspondingly. We then plug these estimators into Eq. (35) to produce the corresponding one-step-ahead predicted value for each of the time series. For further details on the CLS method, the reader is referred to Section B. The SPP assumes, for a single time series, the observed counts are independent identically distributed Poisson random variables with a constant rate value, λ . Therefore, we estimate λ for each time series using its corresponding counts average and then use this as the one-step-ahead predictor.

To evaluate the different methodologies we use root mean square error (RMSE) and absolute percentage error (APE) between the true population expected value and its corresponding estimated value based on the $L = 100$ time series. The results of this analysis are presented in Table 3. The analysis reveals that our method consistently yields more accurate results compared to the CLS method and the SPP. As expected, the better the separation between the cluster rate values, the easier it is for our method to estimate the parameters more accurately. In addition, generally higher autocorrelation values produce lower APE but

Thin	0.1			0.5			0.9		
Rates	Easy	Med	Hard	Easy	Med	Hard	Easy	Med	Hard
SPP RMSE	0.477	0.113	0.005	1.674	0.880	0.293	6.128	1.155	0.552
CLS RMSE	0.306	0.080	0.035	0.284	0.114	0.057	0.343	0.118	0.055
BNP RMSE	0.219	0.058	0.026	0.260	0.086	0.045	0.299	0.075	0.043
SPP APE	0.067	0.159	0.1241	0.1958	0.3192	0.2013	0.1230	0.3372	0.2737
CLS APE	0.041	0.142	0.110	0.024	0.120	0.093	0.006	0.090	0.047
BNP APE	0.033	0.041	0.072	0.019	0.033	0.044	0.005	0.046	0.022
$E(y_{T+1})$	5.383	1.001	0.317	9.861	1.848	0.591	52.161	9.908	3.0633

Table 3: Conditional mean estimation comparison between the CLS, SPP and our Bayesian nonparametric (BNP) method. The first four rows show the mean square error (MSE) and the absolute percentage error (APE) between the population (true) one-step-ahead conditional mean and its corresponding estimated value. The last row shows the average population (true) conditional expected value.

higher RMSE. Intuitively because the stationary distribution mean value for the PoINAR(1) process is $\mathbb{E}(y) = \frac{\lambda}{1-\alpha}$, higher autocorrelation, α , yields a higher marginal mean value (or alternatively higher count values). This indicates a larger separation between the clusters counts values for the data sets with higher α . Therefore, higher autocorrelation helps our method identify the “true” clusters and yield more accurate estimators based on shrinking.

In conclusion, we believe that because the CLS and SPP methods consider each time series separately, they are more prone to over-fitting. The proposed Bayesian methodology allows the estimates to pool information from several time series resulting in more robust parameter estimates.

D Washington, D.C. population density map

Figure 13 shows the map of population density across the 188 Washington, D.C. census tracts.

E Washington D.C. crimes time series

Figure 14 shows the time series of weekly counts of violent crimes in four tracts between 2001 and 2008. We again see that some tracts can have very few occurrences whereas others

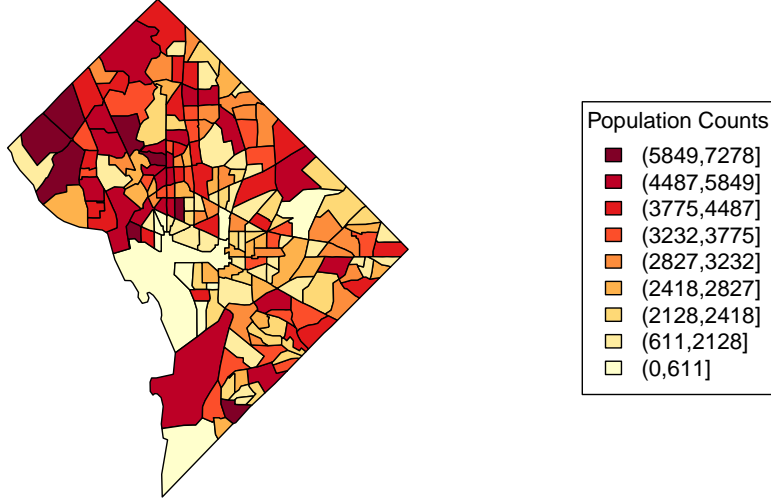


Figure 13: Washington, D.C. map of population density across the 188 census tracts.

$y_{,T}$	0	1	2	3	4	Overall
SPP bias	0.0873 (0.0303)	0.092 (0.0458)	0.2080 (0.095)	0.4730 (0.1761)	0.5308 (0.2434)	0.126 (0.0379)
CLS bias	-0.1625 (0.0383)	-0.0834 (0.0441)	0.1310 (0.0716)	0.3287 (0.1276)	0.3849 (0.3736)	-0.073 (0.0405)
BNP bias	-0.0234 (0.0156)	0.0690 (0.0393)	0.2175 (0.0710)	0.2196 (0.1143)	0.19262 (0.3528)	0.0456 (0.0232)
Frequency	0.5900	0.2340	0.1160	0.0400	0.0200	1

Table 4: One-step-ahead average bias as a function of the last observed value of $y_{,T}$.

have as many as 9 violent crimes per week. Also, since the counts are both discrete and small, it is hard to see clear seasonality within the weekly series.

F Bias analysis

In Table 4, we provide a summary of the average one-week-ahead bias for the Washington, D.C. crime data analysis. As we see from the results, in general, our method produces the smallest bias, but the differences between the methods are not significant except when the last observed count is zero.

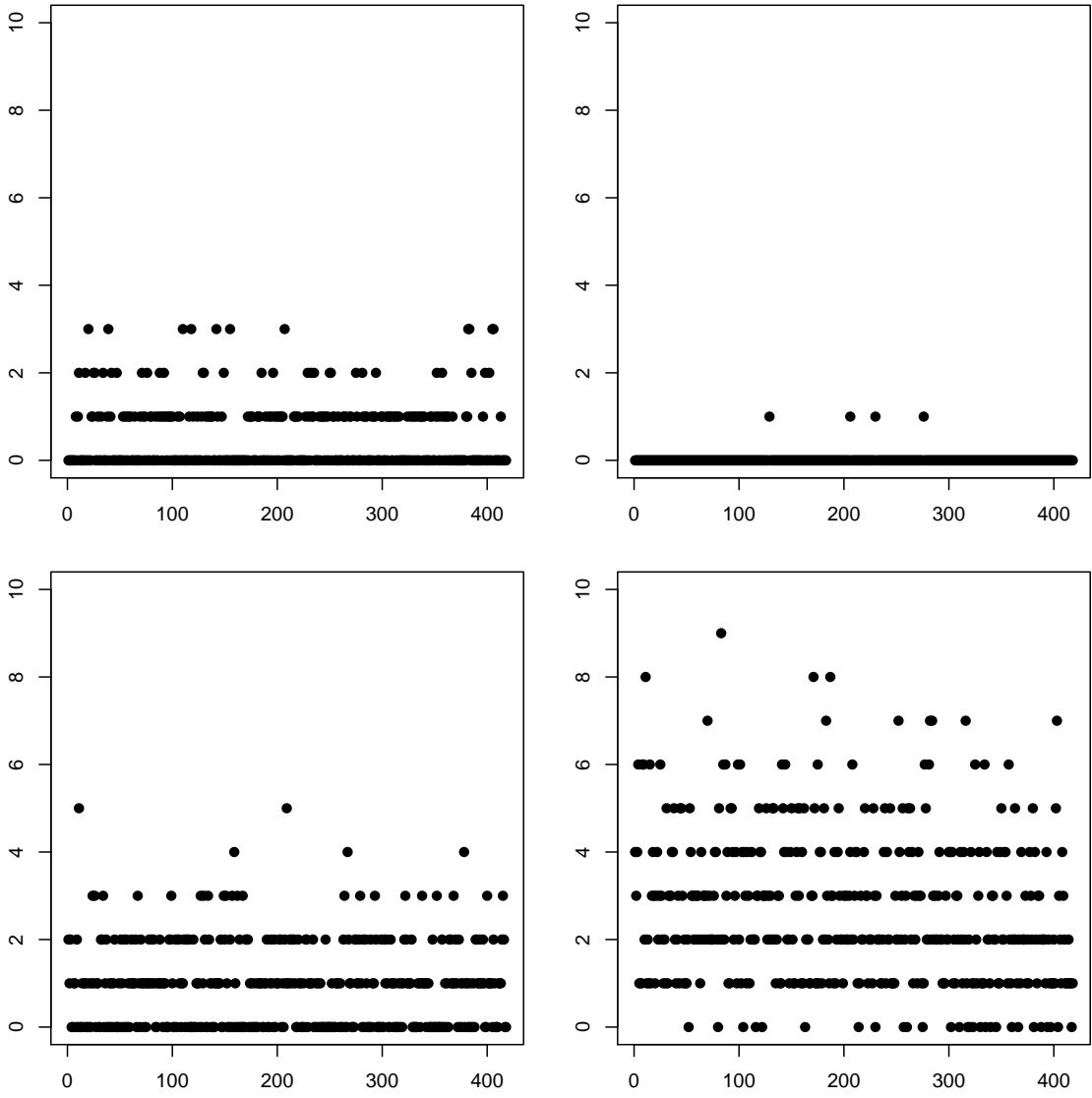


Figure 14: Weekly violent crime counts between 2001 and 2008 in 4 census tracts.